Processes Controlling the Diameter Distribution of Single-Walled Carbon Nanotubes during Catalytic Chemical Vapor Deposition

Matthieu Picher,[†] Eric Anglaret,[†] Raul Arenal,[‡,§] and Vincent Jourdain[†,*]

[†]Laboratoire des Colloïdes, Verres et Nanomatériaux, UMR 5587 CNRS-UM2, University Montpellier 2, Place Bataillon, 34095 Montpellier Cedex 5, France, [‡]Laboratoire d'étude des microstructures, UMR 104 CNRS-ONERA, 29 Avenue de la Division Leclerc, 92322 Châtillon, France, and [§]Laboratorio de microscopias avanzadas (LMA), Instituto de Nanociencia de Aragon (INA), U. Zaragoza, c/Mariano Esquillor s/n, 50018 Zaragoza, Spain

ABSTRACT Single-walled carbon nanotubes are grown by catalytic chemical vapor deposition in various conditions of temperature and carbon precursor pressure. Systematic analyses of the Raman radial breathing modes at two laser wavelengths are used to monitor the evolution of the diameter distribution. Two distinct domains with opposite influences of the temperature and the precursor pressure on the diameter distribution are evidenced. Thanks to specially designed experiments made of two successive growths, three processes are identified to influence the diameter distribution during the nanotube growth: (i) at too low precursor pressure, nanotube nucleation cannot occur on the smallest catalyst particles; (ii) at low temperature and high precursor pressure, small catalyst particles are preferably encapsulated by disordered carbon structures; (iii) at high temperature, catalyst coarsening causes the disappearance of the smallest catalyst particles.

KEYWORDS: carbon nanotubes · SWNT · CVD · Raman · diameter selectivity · nanocatalyst

Catalytic chemical vapor decomposition (CCVD) is presently the most widely used technique for growing single-walled carbon nanotubes (SWNTs). In most synthesis protocols, this process results in a broad SWNT diameter distribution. However, growing nanotube samples with a given chirality is the keypoint for the development of nanotube-based applications in the fields of electronics and optoelectronics. Ultracentrifugation in a gradient density gives promising results for sorting nanotubes by diameter,[1] semiconducting or metallic nature,[2,3] or chirality.[4,5] Up to 79% of a single chirality has been obtained by Chen *et al.*,[5] but this process is complex and partially destructive (wrapping, sonication, ultracentrifugation). Moreover, samples already enriched in a few chiralities are required in order to reach high enrichments.[5] An alternative approach consists of controlling the diameter and/or chirality directly during the growth. The possibility of inducing a strong chiral selectivity during the growth was already demonstrated by Bachilo *et al.* with the CoMoCat process.[6] This process allows one to obtain samples with an especially high percentage of (6,5) and (7,5) nanotubes. More recently, Li *et al.* obtained a very narrow distribution peaked on small diameter and large chiral angles (essentially (6,5), (7,5), and (7,6) SWNTs) by using a bimetallic catalyst FeRu combined to methane at high temperatures.[7] A similar result was obtained by Wang *et al.* with a mixed catalyst CoMo at high CO partial pressures.[8]

A severe control of the SWNT diameters would help to constrain the growth to a few given chiralities with semiconducting nanotubes of close energy gaps. Experimentally, it has been observed that the diameter distribution can be tuned by adjusting the growth parameters. Jeong *et al.*[9] showed that a high density of catalyst nanoparticles favors the growth of nanotubes with large diameters. Furthermore, Lu *et al.*[10] evidenced that an increase of the partial pressure of carbon precursor (ethane) results in larger diameters. As far as the temperature is concerned, other studies suggest a wider diameter distribution associated with an increase of the proportion of large diameters as growth temperature increases.[11−13] By contrast, Kwok *et al.* showed that high temperatures favor carbon nanotubes with both large and small diameters, while lower temperatures favor nanotubes with intermediate sizes.[14] Unfortunately, the few systematic studies reported so far were usually restricted to the influence of only one growth parameter. Consequently, the nature of the processes controlling the distribution of nanotube

* Address correspondence to jourdain@lcvn.univ-montp2.fr.

Received for review December 3, 2010 and accepted February 3, 2011.

Published online February 11, 2011
10.1021/nn1033086

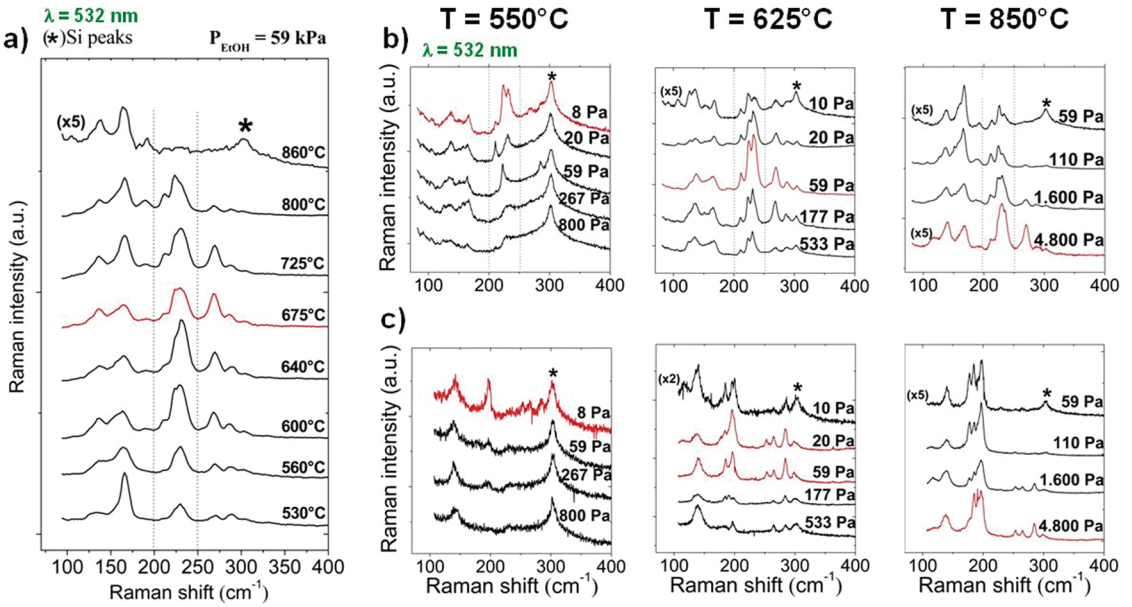

Figure 1. (a) Evolution of the RBM spectra as a function of synthesis temperature (P_{EtOH} = 59 Pa and λ = 532 nm). (b) Evolutions of the RBM spectra as a function of ethanol partial pressure at 550, 625, and 850 °C for an excitation line of 532 nm. (c) Same as (b) for an excitation line of 647 nm. Red curves correspond to the maximal proportion of small diameter nanotubes.

diameter remains an important but still open question.

From a conceptual point of view, several processes can be considered to be involved in the diameter selectivity. The preponderance of some chiralities may first be explained by a higher thermodynamic stability of the corresponding nanotubes and/or nucleation caps.[15] This argument can explain the effect of temperature on the diameter distribution but not the influence of the precursor pressure. A second possible key for selectivity could be a chirality or diameter dependence of the growth kinetics. There are few experimental data on this point: studying individual ultralong nanotubes, Yao *et al.* showed that the growth rate can vary by at least a factor 2 for two different nanotubes in the same synthesis conditions.[16] On the other hand, the size of the catalyst particle is expected to set the higher limit of the nanotube diameter.[17−19] As a consequence, all phenomena influencing the particle size distribution, such as the dewetting of the deposited catalyst layer, Ostwald ripening, and particle coalescence,[20] are expected to strongly influence the final nanotube diameter distribution.

Here, we present a systematic study of the evolution of the SWNT diameter distribution as a function of two growth parameters: the temperature and the precursor partial pressure. Raman spectroscopy was used as characterization technique. Raman spectroscopy is a powerful tool for this study, first because of its high sensitivity to the presence of SWNT due to the Raman resonance effect, and because the frequency of the radial breathing mode (RBM) is inversely proportional to the nanotube diameter.[21] Compared to previous observations, we identify two domains of temperature and partial pressure with opposite influences of the growth parameters on the diameter distribution. We notably report a domain at low temperatures and high pressures where the nanotube distribution shifts to smaller diameters as the temperature increases or the precursor pressure decreases. To identify the phenomena involved in the diameter selection, we performed additional experiments made of two successive growths in a microreactor allowing *in situ* Raman measurements.

RESULTS AND DISCUSSION

Figure 1a displays the evolution of the RBM profiles (λ = 532 nm) of the samples as a function of the temperature *T* in the case of the nickel−ethanol couple. For the sake of clarity, the RBM domain is arbitrarily divided into three regions corresponding to low, intermediate, and high RBM frequencies. One can observe that the relative weight of high frequency RBM, that is, of small SWNT diameters, increases when temperature increases until a threshold value of 675 °C. Above 675 °C, the intensity of high frequency RBM decreases to the benefit of low frequency RBM. The RBM profile is also very dependent on the ethanol partial pressure *P*, as shown in Figure 1b. For each temperature, one can define an optimal ethanol pressure for high frequency RBM. This optimal partial pressure increases with increasing temperatures: 8 Pa at 550 °C, 59 Pa at 625 °C, 4.800 Pa at 800 °C. The same evolutions are observed at the excitation wavelength of 647 nm (Figure 1c). Please note that, at 532 nm, high frequency RBM values are assigned to metallic nanotubes while they are assigned to semiconducting ones at 647 nm based on the values of optical transition energies proposed by Fantini *et al.*[22] Consequently, the changes in the RBM profiles

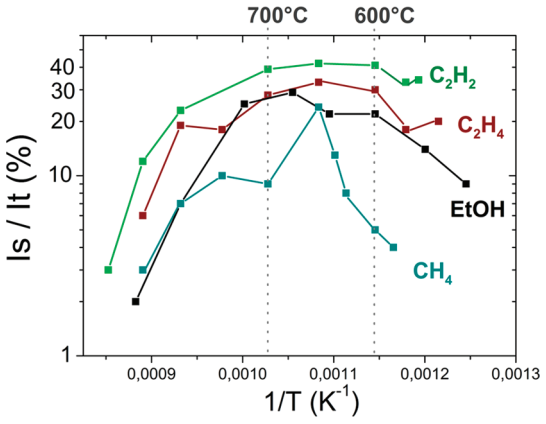

Figure 2. Evolution of the I_S/I_T ratio as a function of the inverse growth temperature for different carbon precursors.

must be interpreted in terms of changes in the diameter distribution and not in the metal/semiconducting ratio.

From these results, one can identify two distinct domains with opposite influences of T and P on the diameter distribution. In the low T—high P domain, increasing the temperature or decreasing the precursor pressure favors the growth of small diameter SWNTs. On the contrary, in the high T—low P domain, the synthesis of small diameter SWNTs is promoted by decreasing the temperature or increasing the precursor pressure. The highest proportions of small diameter SWNTs are obtained at the frontier of the two domains.

Other carbon precursors (methane, acetylene, and ethylene) were used with nickel to check the generality of this behavior. The evolutions of the RBM profiles as a function of temperature for methane, acetylene, and ethylene are presented in Figure S2 (see Supporting Information). For a quantitative comparison of the proportion of small diameter nanotubes, we defined a relative index $S = I_T/I_S$, where I_S corresponds to the peak area of the RBM bunch in the small diameters region above 250 cm^{-1} and I_T corresponds to the total intensity of the RBM peaks. Figure 2 shows the evolution of the I_S/I_T ratio for the different carbon precursors used in this study. One can observe that the behavior observed with ethanol is general to all of the carbon precursors that we investigated. For all of these precursors, the proportion of small diameters peaks for an intermediate temperature ranging between 600 and 700 °C.

It is widely accepted that the diameter of a growing carbon nanotube is primarily controlled by the size of its catalyst particle.[17−19] Other parameters such as the strength of the carbon−metal interaction[23] may also have an influence but can be considered as secondary. For instance, the study of Yao *et al.* demonstrated that the diameter of a growing nanotube could be decreased by 1−6 Å by increasing the growth temperature by 50−100 °C.[24] This effect alone cannot explain

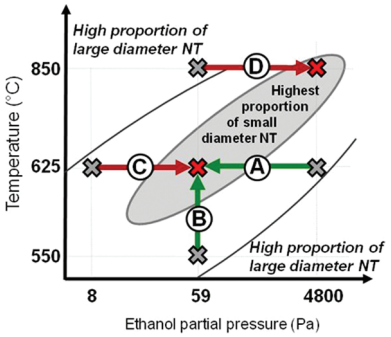

Figure 3. Schematic representation of the evolution of the diameter distribution as a function of temperature and ethanol pressure. Each arrow corresponds to a two-step growth experiment.

the large variations of diameter distribution observed in this work. Considering that the nanotube diameter is primarily controlled by the size of its catalyst particle, three processes can be proposed to explain the lower amount of small diameter nanotubes outside the optimal region: (i) the lack of small particles, (ii) the absence of nucleation on small particles, (iii) the encapsulation of small particles.

In order to identify the acting processes, we devised an experimental protocol based on two successive growths (see Figure 3). The first growth is performed in a region where the proportion of small diameter SWNTs is low (gray crosses). Once no more evolution of the Raman spectrum is observed in the *in situ* measurements, the synthesis is stopped and a first Raman spectrum (labeled as #1) is recorded at room temperature. A second growth is carried out on the same sample, in conditions that are now optimal for small diameters (red crosses). Please note that the sample remains in the controlled environment of the cell during the whole experiment. Once again, a Raman spectrum (labeled as #2a) is recorded at room temperature and at the same position on the sample. The two RBM profiles are compared to the growth directly performed in the conditions optimal for small diameters (labeled as "reference synthesis"). If additional small diameter nanotubes appear between the first and the second growth, it supports that small nanoparticles were present during the former but were not activated. If no small diameter is produced in the second step, we proceed to a new experiment: the same protocol is executed again on a new sample but an oxidizing step (O_2, 700 °C, 5 min) is added between the two growth steps. The oxidizing step allows one to remove all carbonaceous species and to reactivate the encapsulated catalyst particles. As previously, a second Raman spectrum (#2b) is recorded at the end of the second growth. The goal of this experiment is to detect the presence of small nanoparticles that may have been encapsulated by carbonaceous species during the first growth. If small diameters appear during the second step after the oxidation treatment, it supports

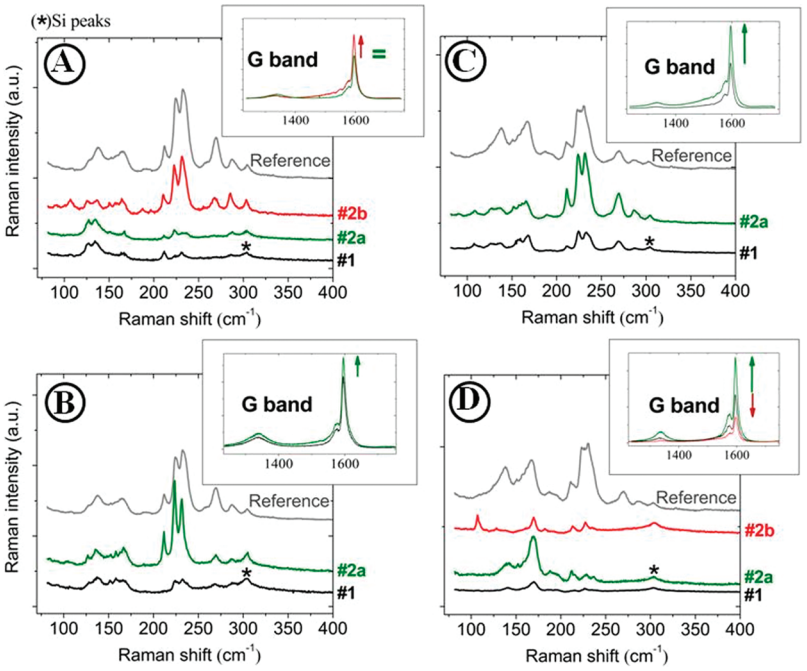

Figure 4. Raman spectra obtained for successive growths experiments. The conditions of each experiment are summarized in Figure 3. Spectrum #1 corresponds to the first growth. Spectra #2a and #2b correspond to the second growth without and with an oxidizing step, respectively. The gray curve labeled as Reference corresponds to a synthesis directly performed in the experimental conditions of #2.

that small nanoparticles were present from the beginning but were deactivated due to encapsulation by carbon species during the first growth. By contrast, if no change is observed in the high frequency range, it supports that the smallest nanoparticles were irreversibly deactivated during the first growth due to catalyst restructuring (Ostwald ripening, coalescence,[20] or diffusion of the catalyst into the silicon support[25−27]). To validate this last protocol, we made sure that the oxidative step does not modify the nanotube diameter distribution by performing two similar syntheses with an oxidation step between (see Figure S3 in Supporting Information).

We first focus on the low temperature−high precursor pressure domain. Experiment A consists of a first growth at T = 625 °C and P_{EtOH} = 1.600 Pa followed by a second growth at smaller P_{EtOH} of 59 Pa, close to the optimal conditions for the growth of small diameters (Figure 3). No extra growth can be observed when the second step is achieved without previous oxidation (spectrum #2a in Figure 4a). By contrast, if the second growth occurs after an oxidative step, the Raman spectrum #2b shows extra peaks of small diameter nanotubes. This experiment supports that the smallest catalyst particles were encapsulated by carbonaceous species during the first step (thus preventing the growth of small diameter SWNTs) and were reactivated by the oxidative treatment between the first and second steps (thus allowing the growth of small diameter SWNTs).

In experiment B, the first synthesis takes place at T = 550 °C and P_{EtOH} = 59 Pa and the second one at 625 °C (see Figure 3 and Figure 4b). Following the increase of temperature, an extra growth of small diameter nanotubes is observed. One can conclude that small catalyst particles were initially not activated but were activated by an increase of temperature. Figure S4 (Supporting Information) shows typical HRTEM micrographs of the samples grown in the low T−high P domain. Catalyst nanoparticles appear embedded into disordered carbon nanostructures. The presence of disordered carbon is also reflected in the peak ratio of the Raman G and D bands. The G/D ratio is proportional to the coherence length of the crystalline domains[28] and is widely used to estimate the density of defects in nanotubes.[14,29,30] The G/D ratio of the samples grown in this domain are much lower than those corresponding to the high T−low P domain (see Figures S1 and S4 in Supporting Information).

These results support that, in the low temperature−high precursor pressure domain, catalyst particles are deactivated due to encapsulation by disordered carbon envelopes. It explains why reactivation can experimentally be achieved by either oxidation or by annealing at a higher temperature: the first treatment induces the combustion of the disordered carbon envelopes, while the second one may either induce a dissolution or a rearrangement of the carbon envelope encapsulating the particle. We propose that the lack of small diameter SWNTs in this domain is explained by a preferable encapsulation of the smallest particles.

We now move to the high temperature−low precursor pressure domain. Experiment C corresponds to a first synthesis at T = 625 °C and P_{EtOH} = 10 Pa followed

by a second synthesis at P_{EtOH} = 59 Pa (Figure 3). The growth of small diameter nanotubes is observed when increasing the partial pressure (spectrum #2a in Figure 4c). Therefore, in this domain, small nanoparticles are not irreversibly deactivated: they can be activated by increasing the partial pressure of carbon precursor. We previously reported that the threshold precursor pressure to initiate nanotube growth increases with temperature,[31] which can be explained by the increased carbon solubility. The Ostwald–Freundlich equation[32,33] relates the solubility of a material to its surface free energy and grain size:

$$\frac{S}{S_0(7)} = \exp\left(\frac{2\gamma V}{RTr}\right)$$

where S is the solubility of grains with radius r, S_0 is the solubility of the bulk material, γ is the surface free energy, V is the molar volume, R is the gas constant, and T is the temperature. The equation stipulates that, as the grain dimension decreases, the solubility increases exponentially relative to the solubility of the bulk material. The solubility is expected to change appreciably only as the radius of a particle enters into the nanoscale. From this relation, one expects a higher supersaturation limit for small catalyst nanoparticles compared to larger ones. This is also in agreement with our observation that the nucleation of small diameter nanotubes requires a higher partial pressure of carbon precursor compared to large diameter ones.

In experiment D, the first synthesis is at T = 850 °C and P_{EtOH} = 59 Pa, and the second one at P_{EtOH} = 1.600 Pa (Figure 3). Without oxidation, no regrowth of small diameter nanotubes is observed (spectrum #2a in Figure 4d). However, the increase of the partial pressure generates the regrowth of large diameter nanotubes. This is associated with an increase of the G band, which is indicative of the overall nanotube yield (see inset in Figure 4d). Even after an oxidation step, one only notes a regrowth of large and intermediate diameters. The oxidation step causes a significant lowering of the final yield. We conclude that, in this high temperature domain, small nanoparticles get irreversibly deactivated.

To explain the partial discrepancy between experiment C performed at 625 °C and experiment D performed at 850 °C, we made additional experiments. In these experiments, the synthesis conditions were the same and correspond to an optimum for small diameter nanotubes (T = 625 °C, P_{EtOH} = 59 Pa). However, the pretreatment was modified compared to our standard protocol. In a first experiment, we performed the argon pretreatment for a longer time (13 min instead of 5 min) and at higher temperature (T = 850 °C instead of 700 °C). In a second experiment, a low pressure of ethanol (P_{EtOH} = 10 Pa) diluted in argon was introduced during the pretreatment instead of pure argon (13 min, T = 850 °C). This ethanol partial pressure is lower than

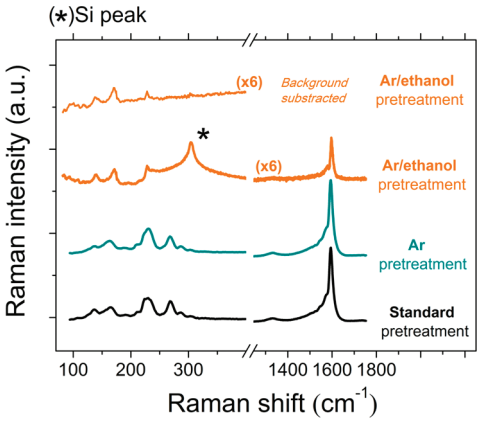

Figure 5. Raman spectra for three syntheses performed at T = 625 °C and P_{EtOH} = 59 Pa with different pretreatments. The black curve corresponds to a standard pretreatment. The blue curve corresponds to a long pretreatment under argon at high temperature (T = 850 °C, 13 min). The orange curve corresponds to pretreatment with ethanol at P_{EtOH} = 10 Pa diluted in argon (T = 850 °C, 13 min).

the threshold partial pressure of nucleation that we previously evidenced[31] and therefore does not allow the growth of carbon structures. The Raman spectra of the samples grown in these experiments are presented in Figure 5. One can observe that, under pure argon, the G band intensities and the RBM profiles remain similar whatever the pretreatment temperature and duration. On the contrary, when a small amount of ethanol is present during the pretreatment, the amount of grown nanotubes is dramatically lowered. In addition, the diameter distribution shifts toward much larger diameters. These experiments support that catalyst particles start coalescing into larger particles once ethanol is introduced. This fast restructuring may be explained by the reduction of the catalyst particles once ethanol is introduced since the atom mobility is much higher in the metallic form than in the oxide state. We previously reported *in situ* measurements showing that oxidized catalyst particles are reduced by ethanol in such conditions.[31]

From these results, catalyst restructuring appears as another source of deactivation that impacts the density of small catalyst particles. The process is dominant at high temperature and for particles in a reduced state. Compared to the previously discussed processes (encapsulation by carbon, absence of nucleation), the resulting state of the catalyst particles cannot be modified by oxidation or an increased precursor pressure. These results provide an explanation for the discrepancy between experiments C and D. In experiment D, increasing the precursor pressure induced the growth of additional nanotubes (spectrum 2a in Figure 4d) but with much less small diameter nanotubes than expected if one considers the RBM profile of the reference synthesis (reference spectrum in Figure 4d). From the results presented in Figure 5, this can be explained by the fast catalyst restructuring at

the high temperature of experiment D. We conclude that, in experiment D, lowering the precursor pressure hampered the formation of small diameter nanotubes for two reasons: (i) as in experiment C at 675 °C, there is no nanotube nucleation on small diameter particles if the precursor pressure is too low (which we attribute to an increase of the carbon solubility as the particle size decreases); (ii) the low *P*—high *T* conditions promote both a fast catalyst coarsening and a slow nanotube growth so that small catalyst particles rapidly vanish at the beginning of nanotube growth.

In the proposed model, the carbon solubility of the nanoparticle dictates the threshold pressure above which the surface concentration of carbon atoms is high enough to allow the nucleation of carbon structures. From our data and in agreement with the Ostwald—Freundlich relation, small nanoparticles have a higher carbon solubility and therefore a higher threshold pressure for the nucleation of carbon structures. Above the threshold pressure, carbon structures are thermodynamically allowed at the particle surface and can lead either to the formation of a nanotube or to the encapsulation of the nanoparticle: high temperature and low carbon supply promote the formation of a well-ordered nanotube, while low temperature and high carbon supply favor the formation of a disordered carbon layer encapsulating the particle. Our experimental data support that small nanoparticles are more affected by this type of encapsulation (which is the predominant deactivation mechanism only at low temperature and high carbon supply). It may seem contradictory that small nanoparticles that have a higher carbon solubility are more impacted by carbon encapsulation. However, this argument supposes that the particle rapidly reaches the thermodynamic equilibrium at the time scale of nanotube nucleation (*i.e.*, that bulk diffusion of carbon atoms is much faster than the supply of carbon atoms from the gas phase). In conditions of low temperature and high precursor pressure, this may not be the case, which would explain why the carbon solubility of the particle has no or little influence on the particle encapsulation. Other arguments can be suggested to explain why small particles are more affected by the encapsulation by a disordered carbon layer. The binding energy of atoms and molecules to metal nanoparticles is dependent on the cluster size[34] which has implications on their catalytic activity.[35] It may be that the decomposition of the carbon precursor is faster on small particles, leading to a higher risk of encapsulation. Alternatively, if the carbon—metal binding energy is strongly dependent on the cluster size, surface diffusion of carbon atoms may be slower at the surface of small particles, also leading to their preferential encapsulation. Quantum-based molecular dynamics simulations for different cluster sizes could help answering this question.

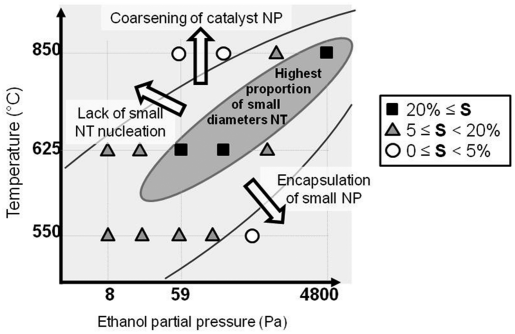

Figure 6. Small diameter index *S* as a function of temperature and ethanol partial pressure for the Ni—ethanol couple. The processes influencing the nanotube diameter distribution in each domain are presented.

The kinetics and thermodynamics of the three identified processes (encapsulation by excessive carbon, nanotube nucleation, and catalyst coarsening) are dependent on the nature of the catalyst and so should be their relative influence on the diameter distribution. For instance, Mattevi *et al.*[36] reported that, due its higher interactions with the oxide support, iron should be less affected than nickel by catalyst coarsening. The critical carbon concentration for nanotube nucleation is expected to be higher for iron nanoparticles compared to nickel ones due to the higher carbon solubility of bulk iron.[37] Numerical simulations also support that, due to higher adhesion energy, iron nanoparticles are more sensitive to carbon encapsulation than nickel ones.[38] Our results support that, in the general case, more than one regime should be *a priori* expected. However, some catalytic systems may experimentally display one regime only because they permit SWNT growth in only a narrow range of growth parameters.

CONCLUSION

In summary, two distinct domains with opposite influences of the temperature and the precursor pressure on the diameter distribution were evidenced. The observation of two regimes for the studied systems is important for the understanding of the processes involved in nanotube growth and for the development of a general growth model. On the basis of the results of two-step experiments, three processes were identified, as summarized in Figure 6, showing the proportion of small diameter nanotubes as a function of *T* and *P*. In the low *T*—high *P* domain, the growth of small diameters nanotubes can be activated by burning away the carbon deposits or by increasing the temperature. We propose that this behavior originates from an encapsulation of the catalyst particles by disordered carbon envelopes that were evidenced by HRTEM. It was previously reported that such an encapsulation is favored at low temperatures and high precursor pressures.[39] From this study, it appears that the small catalyst particles are more efficiently encapsulated than the

big ones. In the high *T*—low *P* domain, the growth of small diameter nanotubes can be activated by increasing the precursor pressure. This supports that small catalyst particles have a higher supersaturation limit than larger particles, as theoretically expected from the Ostwald—Freundlich relation. This attribution is further supported by the fact that the threshold precursor pressure increases with temperature.[31] Finally, an additional phenomenon causing an irreversible deactivation of the smallest catalyst particles is observed at high temperature. The phenomenon is accelerated when introducing the carbon precursor. We attribute this behavior to the restructuring of the catalyst nanoparticles by Ostwald ripening or coalescence. In this high temperature domain, the nanotube diameter distribution apparently results from the kinetic competition between the nanotube growth and the catalyst coarsening.

MATERIALS AND METHODS

Ethanol was used as carbon precursor, and a thin layer of nickel deposited on SiO_2/Si substrates was used as catalyst using a previously reported protocol.[39] Briefly, CCVD experiments were achieved in a cold-wall CVD microreactor (Linkam TS-1500 stage) equipped with a resistive heating crucible, an integrated thermocouple, and a quartz window allowing *in situ* Raman measurements. Ethanol vapor was supplied into the reactor by bubbling argon (air liquid class 2, 99.996%) through a thermostatted ethanol flask (Fluka, 99.8%) kept at 0 or 25 °C. Saturating ethanol vapor pressures are extratcted from experimental tables. An additional diluting argon line was used to precisely adjust the ethanol partial pressure between 2 Pa and 5 kPa. In the case of other precursors, the partial pressure was controlled by diluting the precursor with argon flow. For all precursors, the total flow was set to 1400 sccm. Thin layers (5 Å) of nickel deposited by evaporation onto (100) silicon substrates with a 100 nm thermal oxide layer were used as catalysts. The substrates were subjected to oxygen pretreatment from room temperature to 700 °C at a rate of 50 °C/min. The cell was then purged with argon for 10 min while reaching the desired synthesis temperature. The ethanol/argon flow was introduced into the reactor, and the growth was followed by *in situ* Raman measurements as reported previously.[39] The synthesis was stopped when the G band typical of SWNTs was stable. The duration of a synthesis went from 1 to 20 min. Finally, the cell was purged with argon and quickly cooled to room temperature (100 °C/min). Postgrowth characterization of the samples by Raman spectroscopy, HRTEM, and SEM evidenced the growth of a thin layer of entangled SWNTs.[39] Raman spectra were recorded with a micro-Raman spectrometer (Jobin Yvon T-64000) equipped with a liquid nitrogen cooled CCD camera. A 532 nm solid laser source (cw diode pumped millennia pro S-series) was precisely focused onto the center of the substrate using a 50× objective lens (1 μm spot size). All of the spectra were recorded in the cell, without exposure to the air and at room temperature. Additional Raman measurements were also achieved using an excitation line at 647 nm. TEM grids were prepared by scratching the surface of a substrate with a diamond tip and collecting the detached substrate pieces on a holey carbon grid. High-resolution transmission electron microscopy (HRTEM) has been performed using three different field-emission TEMs: a Zeiss Libra 200FE (operating at 200 kV) and two FEI Tecnai F20 and F30 (working at 200 and 80 kV, respectively).

Acknowledgment. The authors acknowledge financial support from the Agence Nationale de la Recherche (P3N project "SOS Nanotubes" ANR-09-NANO-028). V.J. acknowledges the support of CNRS and University Montpellier 2 for a research sabbatical (délégation CNRS). The authors thank Saïd Tahir, David Maurin, Frédéric Pichot, and Eric Alibert for technical assistance.

Supporting Information Available: Temperature dependence of the G band and G/D ratio, RBM profiles for various precursors and additional Raman, SEM and HRTEM data are presented. This material is available free of charge *via* the Internet at http://pubs.acs.org.

REFERENCES AND NOTES

1. Arnold, M.; Stupp, S.; Hersam, M. Enrichment of Single-Walled Carbon Nanotubes by Diameter in Density Gradients. *Nano Lett.* **2005,** *5*, 713–718.
2. Arnold, M.; Green, A.; Hulvat, J.; Stupp, S.; Hersam, M. Sorting Carbon Nanotubes by Electronic Structure Using Density Differentiation. *Nat. Nanotechnol.* **2006,** *1*, 60–65.
3. Strano, M.; Dyke, C.; Usrey, M.; Barone, P.; Allen, M.; Shan, H.; Kittrell, C.; Hauge, R.; Tour, J.; Smalley, R. Electronic Structure Control of Single-Walled Carbon Nanotube Functionalization. *Science* **2003,** *301*, 1519.
4. Nish, A.; Hwang, J.; Doig, J.; Nicholas, R. Highly Selective Dispersion of Single-Walled Carbon Nanotubes Using Aromatic Polymers. *Nat. Nanotechnol.* **2007,** *2*, 640–646.
5. Chen, F.; Wang, B.; Chen, Y.; Li, L. Toward the Extraction of Single Species of Single-Walled Carbon Nanotubes Using Fluorene-Based Polymers. *Nano Lett.* **2007,** *7*, 3013–3017.
6. Bachilo, S.; Balzano, L.; Herrera, J.; Pompeo, F.; Resasco, D.; Weisman, R. Narrow (*n*, *m*) Distribution of Single-Walled Carbon Nanotubes Grown Using a Solid Supported Catalyst. *J. Am. Chem. Soc.* **2003,** *125*, 11186–11187.
7. Li, X.; Tu, X.; Zaric, S.; Welsher, K.; Seo, W.; Zhao, W.; Dai, H. Selective Synthesis Combined with Chemical Separation of Single-Walled Carbon Nanotubes for Chirality Selection. *J. Am. Chem. Soc.* **2007,** *129*, 15770–15771.
8. Wang, B.; Wei, L.; Yao, L.; Li, L.; Yang, Y.; Chen, Y. Pressure-Induced Single-Walled Carbon Nanotube (*n*, *m*) Selectivity on Co-Mo Catalysts. *J. Phys. Chem. C* **2007,** *111*, 14612.
9. Jeong, G.; Suzuki, S.; Kobayashi, Y.; Yamazaki, A.; Yoshimura, H.; Homma, Y. Effect of Nanoparticle Density on Narrow Diameter Distribution of Carbon Nanotubes and Particle Evolution during Chemical Vapor Deposition Growth. *J. Appl. Phys.* **2005,** *98*, 124311.
10. Lu, C.; Liu, J. Controlling the Diameter of Carbon Nanotubes in Chemical Vapor Deposition Method by Carbon Feeding. *J. Phys. Chem. B* **2006,** *110*, 20254–20257.
11. Ago, H.; Imamura, S.; Okazaki, T.; Saito, T.; Yumura, M.; Tsuji, M. CVD Growth of Single-Walled Carbon Nanotubes with Narrow Diameter Distribution over Fe/MgO Catalyst and Their Fluorescence Spectroscopy. *J. Phys. Chem. B* **2005,** *109*, 10035–10041.
12. Zhou, W.; Ooi, Y.; Russo, R.; Papanek, P.; Luzzi, D.; Fischer, J.; Bronikowski, M.; Willis, P.; Smalley, R. Structural Characterization and Diameter-Dependent Oxidative Stability of Single Wall Carbon Nanotubes Synthesized by the Catalytic Decomposition of CO. *Chem. Phys. Lett.* **2001,** *350*, 6–14.
13. Alvarez, W.; Pompeo, F.; Herrera, J.; Balzano, L.; Resasco, D. Characterization of Single-Walled Carbon Nanotubes (SWNTs) Produced by CO Disproportionation on Co-Mo Catalysts. *Chem. Mater.* **2002,** *14*, 1853–1858.
14. Kwok, C.; Reizman, B.; Agnew, D.; Sandhu, G.; Weistroffer, J.; Strano, M.; Seebauer, E. Temperature and Time Dependence Study of Single-Walled Carbon Nanotube Growth by Catalytic Chemical Vapor Deposition. *Carbon* **2010,** *48*, 1279–1288.
15. Reich, S.; Li, L.; Robertson, J. Structure and Formation Energy of Carbon Nanotube Caps. *Phys. Rev. B* **2005,** *72*, 165423.

16. Yao, Y.; Liu, R.; Zhang, J.; Jiao, L.; Liu, Z. Raman Spectral Measuring of the Growth Rate of Individual Single-Walled Carbon Nanotubes. *J. Phys. Chem. C* **2007,** *111*, 8407–8409.
17. Lin, M.; Tan, J.; Boothroyd, C.; Loh, K.; Tok, E.; Foo, Y. Direct Observation of Single-Walled Carbon Nanotube Growth at the Atomistic Scale. *Nano Lett.* **2006,** *6*, 449–452.
18. Rodríguez-Manzo, J.; Terrones, M.; Terrones, H.; Kroto, H.; Sun, L.; Banhart, F. *In Situ* Nucleation of Carbon Nanotubes by the Injection of Carbon Atoms into Metal Particles. *Nat. Nanotechnol.* **2007,** *2*, 307–311.
19. Nishimura, K.; Okazaki, N.; Pan, L.; Nakayama, Y. *In Situ* Study of Iron Catalysts for Carbon Nanotube Growth Using X-ray Diffraction Analysis. *Jpn. J. Appl. Phys.* **2004,** *43*, 471–474.
20. Amama, P.; Pint, C.; McJilton, L.; Kim, S.; Stach, E.; Murray, P.; Hauge, R.; Maruyama, B. Role of Water in Super Growth of Single-Walled Carbon Nanotube Carpets. *Nano Lett.* **2008,** *9*, 44–49.
21. Dresselhaus, M.; Dresselhaus, G.; Saito, R.; Jorio, A. Raman Spectroscopy of Carbon Nanotubes. *Phys. Rep.* **2005,** *409*, 47–99.
22. Fantini, C.; Jorio, A.; Souza, M.; Strano, M.; Dresselhaus, M.; Pimenta, M. Optical Transition Energies for Carbon Nanotubes from Resonant Raman Spectroscopy: Environment and Temperature Effects. *Phys. Rev. Lett.* **2004,** *93*, 147406.
23. Ding, F.; Larsson, P.; Larsson, J.; Ahuja, R.; Duan, H.; Rosén, A.; Bolton, K. The Importance of Strong Carbon−Metal Adhesion for Catalytic Nucleation of Single-Walled Carbon Nanotubes. *Nano Lett.* **2008,** *8*, 463–468.
24. Yao, Y.; Dai, X.; Liu, R.; Zhang, J.; Liu, Z. Tuning the Diameter of Single-Walled Carbon Nanotubes by Temperature-Mediated Chemical Vapor Deposition. *J. Phys. Chem. C* **2009,** *113*, 13051–13059.
25. Kim, S.; Pint, C.; Amama, P.; Zakharov, D.; Hauge, R.; Maruyama, B.; Stach, E. Evolution in Catalyst Morphology Leads to Carbon Nanotube Growth Termination. *J. Phys. Chem. Lett.* **2010,** *1*, 918–922.
26. Homma, Y.; Kobayashi, Y.; Ogino, T.; Takagi, D.; Ito, R.; Jung, Y.; Ajayan, P. Role of Transition Metal Catalysts in Single-Walled Carbon Nanotube Growth in Chemical Vapor Deposition. *J. Phys. Chem. B* **2003,** *107*, 12161–12164.
27. Jeong, G.; Yamazaki, A.; Suzuki, S.; Kobayashi, Y.; Homma, Y. Behavior of Catalytic Nanoparticles during Chemical Vapor Deposition for Carbon Nanotube Growth. *Chem. Phys. Lett.* **2006,** *422*, 83–88.
28. Cançado, L.; Takai, K.; Enoki, T.; Endo, M.; Kim, Y.; Mizusaki, H.; Jorio, A.; Coelho, L.; Magalhaes-Paniago, R.; Pimenta, M. General Equation for the Determination of the Crystallite Size L of Nanographite by Raman Spectroscopy. *Appl. Phys. Lett.* **2006,** *88*, 163106–163106.
29. Vinten, P.; Lefebvre, J.; Finnie, P. Kinetic Critical Temperature and Optimized Chemical Vapor Deposition Growth of Carbon Nanotubes. *Chem. Phys. Lett.* **2009,** *469*, 293–297.
30. Yasuda, S.; Hiraoka, T.; Futaba, D.; Yamada, T.; Yumura, M.; Hata, K. Existence and Kinetics of Graphitic Carbonaceous Impurities in Carbon Nanotube Forests To Assess the Absolute Purity. *Nano Lett.* **2009,** *9*, 769–773.
31. Picher, M.; Anglaret, E.; Jourdain, V. High Temperature Activation and Deactivation of Single-Walled Carbon Nanotube Growth Investigated by *In Situ* Raman Measurements. *Diamond Relat. Mater.* **2010,** *19*, 581–585.
32. Hochella, M. There's Plenty of Room at the Bottom: Nanoscience in Geochemistry. *Geochim. Cosmochim. Acta* **2002,** *66*, 735–743.
33. Stöber, W.; Arnold, M. Anomalien bei der Ablösung von KieselsAure von der OberflAche Feinkörniger Siliziumdioxydpulver. *Kolloid-Z.* **1961,** *174*, 20–27.
34. Lang, S.; Bernhardt, T.; Barnett, R.; Landman, U. Size Dependent Binding Energies of Methane to Small Gold Clusters. *ChemPhysChem* **2010,** *11*, 1570–1577.
35. Herranz, T.; Deng, X.; Cabot, A.; Alivisatos, P.; Liu, Z.; Soler-Illia, G.; Salmeron, M. Reactivity of Au Nanoparticles Supported over SiO_2 and TiO_2 Studied by Ambient Pressure Photoelectron Spectroscopy. *Catal. Today* **2009,** *143*, 158–166.
36. Mattevi, C.; Wirth, C.; Hofmann, S.; Blume, R.; Cantoro, M.; Ducati, C.; Cepek, C.; Knop-Gericke, A.; Milne, S.; Castellarin-Cudia, C. *In-Situ* X-ray Photoelectron Spectroscopy Study of Catalyst- Support Interactions and Growth of Carbon Nanotube Forests. *J. Phys. Chem. C* **2008,** *112*, 12207–12213.
37. Yokoyama, H.; Numakura, H.; Koiwa, M. The Solubility and Diffusion of Carbon in Palladium. *Acta Mater.* **1998,** *46*, 2823–2830.
38. Page, A.; Minami, S.; Ohta, Y.; Irle, S.; Morokuma, K. Comparison of Single-Walled Carbon Nanotube Growth from Fe and Ni Nanoparticles Using Quantum Chemical Molecular Dynamics Methods. *Carbon* **2010,** *48*, 3014–3026.
39. Picher, M.; Anglaret, E.; Arenal, R.; Jourdain, V. Self-Deactivation of Single-Walled Carbon Nanotube Growth Studied by *In Situ* Raman Measurements. *Nano Lett.* **2009,** *9*, 542–547.